

2

**AD-A239 301**



**The Influence of Fermi-Level Pinning at  
the GaAs Substrate on HEMT Threshold Voltage**

Prepared by

**R. J. KRANTZ, D. C. MAYER, and W. L. BLOSS**  
Electronics Research Laboratory  
Laboratory Operations  
The Aerospace Corporation  
El Segundo, CA 90245

1 April 1991

**DTIC**  
**ELECTE**  
**AUG 5 1991**  
**S B D**

Prepared for

**SPACE SYSTEMS DIVISION**  
**AIR FORCE SYSTEMS COMMAND**  
Los Angeles Air Force Base  
P.O. Box 92960  
Los Angeles, CA 90009-2960

**THE AEROSPACE CORPORATION**  
El Segundo, California

APPROVED FOR PUBLIC RELEASE;  
DISTRIBUTION UNLIMITED

**91-06800**

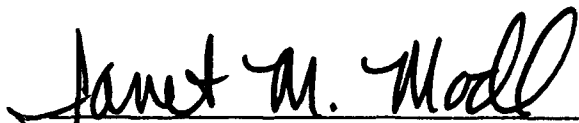


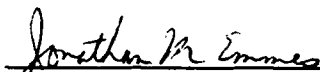
**91 8 01 018**

This report was submitted by The Aerospace Corporation, El Segundo, CA 90245-4691, under Contract No. F04701-88-C-0089 with the Space Systems Division, P.O. Box 92960, Los Angeles, CA 90009-2960. It was reviewed and approved for The Aerospace Corporation by M. J. Daugherty, Director, Electronics Research Laboratory. Captain Janet Modl was the project officer for the Mission-Oriented Investigation and Experimentation (MOIE) Program.

This report has been reviewed by the Public Affairs Office (PAS) and is releasable to the National Technical Information Service (NTIS). At NTIS, it will be available to the general public, including foreign nationals.

This technical report has been reviewed and is approved for publication. Publication of this report does not constitute Air Force approval of the report's findings or conclusions. It is published only for the exchange and stimulation of ideas.

  
JANET MODL, CAPT, USAF  
MOIE Project Officer  
STC/SWL

  
JONATHAN M. EMMES, Maj, USAF  
MOIE Program Manager  
AFSTC/WCO OL-AB

UNCLASSIFIED

SECURITY CLASSIFICATION OF THIS PAGE

## REPORT DOCUMENTATION PAGE

1a. REPORT SECURITY CLASSIFICATION <u>Unclassified</u>			1b. RESTRICTIVE MARKINGS		
2a. SECURITY CLASSIFICATION AUTHORITY			3. DISTRIBUTION/AVAILABILITY OF REPORT  Approved for public release; distribution unlimited		
2b. DECLASSIFICATION/DOWNGRADING SCHEDULE			5. MONITORING ORGANIZATION REPORT NUMBER(S) SSD-TR-91-16		
4. PERFORMING ORGANIZATION REPORT NUMBER(S) TR-0089(4925-01)-1			7a. NAME OF MONITORING ORGANIZATION Space Systems Division		
6a. NAME OF PERFORMING ORGANIZATION The Aerospace Corporation Laboratory Operations		6b. OFFICE SYMBOL (If applicable)		7b. ADDRESS (City, State, and ZIP Code) Los Angeles Air Force Base Los Angeles, CA 90009-2960	
6c. ADDRESS (City, State, and ZIP Code) El Segundo, CA 90245-4691		8b. OFFICE SYMBOL (If applicable)		9. PROCUREMENT INSTRUMENT IDENTIFICATION NUMBER F04701-88-C-0089	
8a. NAME OF FUNDING/SPONSORING ORGANIZATION		8c. ADDRESS (City, State, and ZIP Code)		10. SOURCE OF FUNDING NUMBERS	
				PROGRAM ELEMENT NO.	PROJECT NO.
				TASK NO.	WORK UNIT ACCESSION NO.
11. TITLE (Include Security Classification) The Influence of Fermi-Level Pinning at the GaAs Substrate on HEMT Threshold Voltage					
12. PERSONAL AUTHOR(S) Krantz, Richard J.; Mayer, Donald C.; and Bloss, Walter L.					
13a. TYPE OF REPORT		13b. TIME COVERED FROM _____ TO _____		14. DATE OF REPORT (Year, Month, Day) 1 April 1991	
				15. PAGE COUNT 28	
16. SUPPLEMENTARY NOTATION.					
17. COSATI CODES			18. SUBJECT TERMS (Continue on reverse if necessary and identify by block number)		
FIELD	GROUP	SUB-GROUP			
19. ABSTRACT (Continue on reverse if necessary and identify by block number)					
<p>A two-dimensional quantum well, strong-inversion model of threshold in AlGaAs/GaAs high-electron-mobility transistors (HEMTs) has been extended to include the effects of Fermi-level pinning at the semi-insulating boundary results from an abundance of mid-gap traps in the substrate and couples the carrier channel at the AlGaAs/GaAs interface to the substrate. This communication between the carrier channel and the substrate causes the threshold voltage characteristics of the pinned devices to be substantially different from those of a conventional, semi-infinite HEMT structure. The discrepancy in the threshold voltage approaches 250 mV for a 0.1 <math>\mu\text{m}</math> active-layer device having a typical acceptor doping of <math>\sim 10^{14} \text{ cm}^{-3}</math>.</p> <p>The quantum-well HEMT threshold model has also been compared to a classical analysis of the threshold voltage. For low acceptor doping and thin GaAs layers (<math>&lt; 0.5 \mu\text{m}</math>), neglecting quantum effects can result in significant errors in the threshold voltage calculation. For</p>					
20. DISTRIBUTION/AVAILABILITY OF ABSTRACT <input type="checkbox"/> UNCLASSIFIED/UNLIMITED <input type="checkbox"/> SAME AS RPT. <input type="checkbox"/> DTIC USERS			21. ABSTRACT SECURITY CLASSIFICATION Unclassified		
22a. NAME OF RESPONSIBLE INDIVIDUAL			22b. TELEPHONE (Include Area Code)		22c. OFFICE SYMBOL

UNCLASSIFIED

SECURITY CLASSIFICATION OF THIS PAGE

19. ABSTRACT (Continued)

state-of-the-art AlGaAs/GaAs microcircuits, in which device dimensions are shrinking and unintentional acceptor densities are decreasing, analyses of the I-V characteristics of thin, fully depleted devices must be carried out in the electric quantum limit and include the effects of the semi-insulating substrate.

SECURITY CLASSIFICATION OF THIS PAGE

UNCLASSIFIED

## CONTENTS

1.	INTRODUCTION.....	5
2.	SINGLE-SUBBAND, QUANTUM-MECHANICAL HEMT THRESHOLD VOLTAGE.....	11
3.	THRESHOLD VOLTAGE.....	13
3.1	Conventional HEMT.....	13
3.2	Comparison with Thin, Fully Depleted HEMT.....	14
4.	COMPARISON WITH A CLASSICAL ANALYSIS OF MOSFET/THRESHOLD.....	19
5.	SHAPE OF THE CONDUCTION BAND.....	23
6.	SUMMARY.....	27
	REFERENCES.....	29



<b>Accession For</b>	
NTIS GRA&I	<input checked="" type="checkbox"/>
DTIC TAB	<input type="checkbox"/>
Unannounced	<input type="checkbox"/>
Justification	
By	
Distribution/	
<b>Availability Codes</b>	
Dist	Avail and/or Special
A-1	

## FIGURES

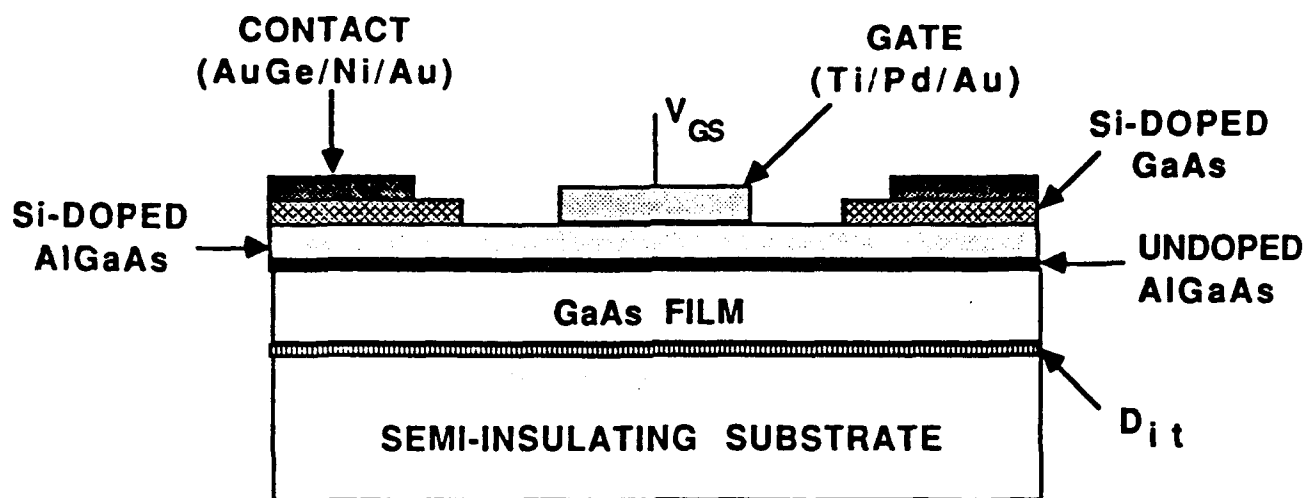
1.	Schematic Cross-Section of (a) a Typical AlGaAs/GaAs HEMT and (b) a Typical SOI MOSFET.....	6
2.	Band Diagram of (a) a Conventional Thick GaAs Film AlGaAs/GaAs HEMT and (b) a Thin GaAs Film AlGaAs/GaAs HEMT Terminated on a Semi-Insulating Substrate.....	7
3.	HEMT Threshold Voltage Difference [Unpinned Minus Pinned] vs Acceptor Density.....	15
4.	The Maximum GaAs Active-Layer Width $W_{max}$ (for Which the Carrier Channel is Coupled to the Back Semi-Insulating Surface) vs Acceptor Density.....	17
5.	Difference in HEMT Threshold Voltage [Unpinned Minus Pinned] vs Acceptor Density for Various GaAs Active-Layer Thicknesses.....	18
6.	Difference in HEMT Threshold Voltage [Unpinned Minus Pinned] vs GaAs Active-Layer Width for Various Acceptor Densities.....	18
7.	Difference in HEMT Threshold Voltage [Unpinned Minus Pinned] vs GaAs Active-Layer Thickness in the Pinned Structure.....	21
8.	The Conduction-Band Edge Relative to the Fermi Level vs Relative Position in the Active Layer for Various Active-Layer Widths and Acceptor Densities of $1 \times 10^{16} \text{ cm}^{-3}$ .....	24
9.	The Conduction-Band Edge Relative to the Fermi Level vs Relative Position in the Active Layer for Various Active-Layer Widths and Acceptor Densities of $1 \times 10^{12} \text{ cm}^{-3}$ .....	24
10.	The Conduction-Band Edge Relative to the Fermi Level vs Relative Position in the Active Layer for the $0.8 \mu\text{m}$ Structure and Various Acceptor Dopings.....	26

## 1. INTRODUCTION

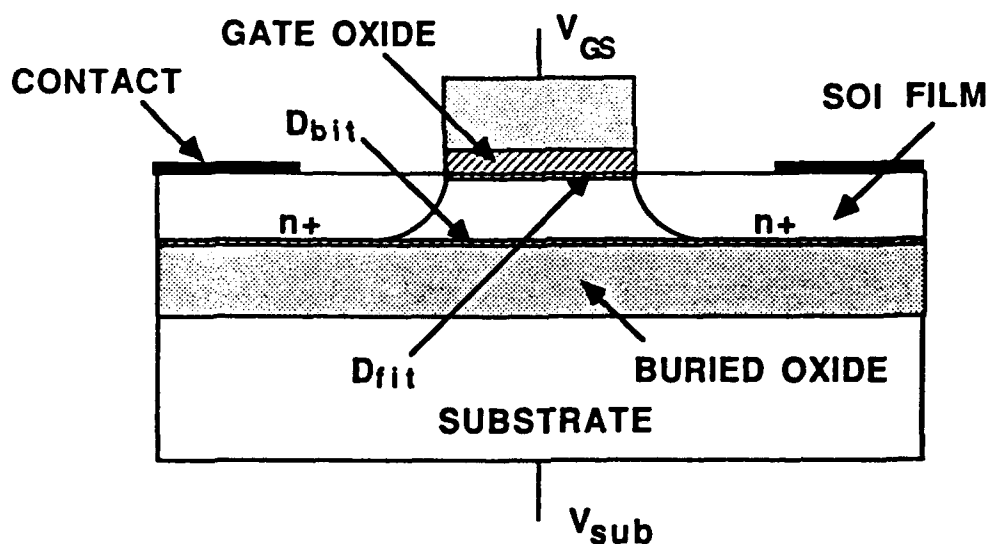
Recent developments in the modeling of high-electron-mobility transistor (HEMT) threshold characteristics [1-3] have pointed out limitations in the original charge control model [4]. One limitation of the original threshold analysis is that it neglected the charge in the depleted portion of the GaAs film compared to the presumably much larger channel charge. However, it has been shown that the depletion-layer charge is larger than the channel charge at threshold [2]. Furthermore, subsequent HEMT models [5-14] have included the additional assumption that the GaAs active layer is large compared to the depletion width. This assumption implies that the electric field at the edge of the depletion region is zero and that the two-dimensional high-mobility conducting channel at the AlGaAs/GaAs interface is decoupled from the effects of the back semi-insulating interface. However, for state-of-the-art HEMTs, these conditions also do not apply.

In SOS/SOI structures the effect of the back interface on device threshold characteristics has been studied extensively [15-22]. Shown in Figures 1a and 1b are schematic cross sections of a typical SOI MOSFET and an AlGaAs/GaAs HEMT. The similarities between the structures are striking. Both consist of a metal gate electrode separated from a conducting film of finite thickness by a nonconducting film of dissimilar material. Each device is fabricated over an insulating substrate which creates a back interface that may affect the electrical behavior of the surface transistor. Because the thickness of the active layer in the AlGaAs/GaAs HEMT is comparable to thicknesses known to affect the surface electrical properties of SOS/SOI MOSFET structures, we have undertaken a study of the effect of the finite active-layer thickness on HEMT threshold properties.

Figures 2a and 2b show the band diagrams of AlGaAs/GaAs HEMTs that have a thick (semi-infinite) GaAs film and a thin GaAs film terminated at the semi-insulating substrate. Both structures are shown under bias  $V_g$

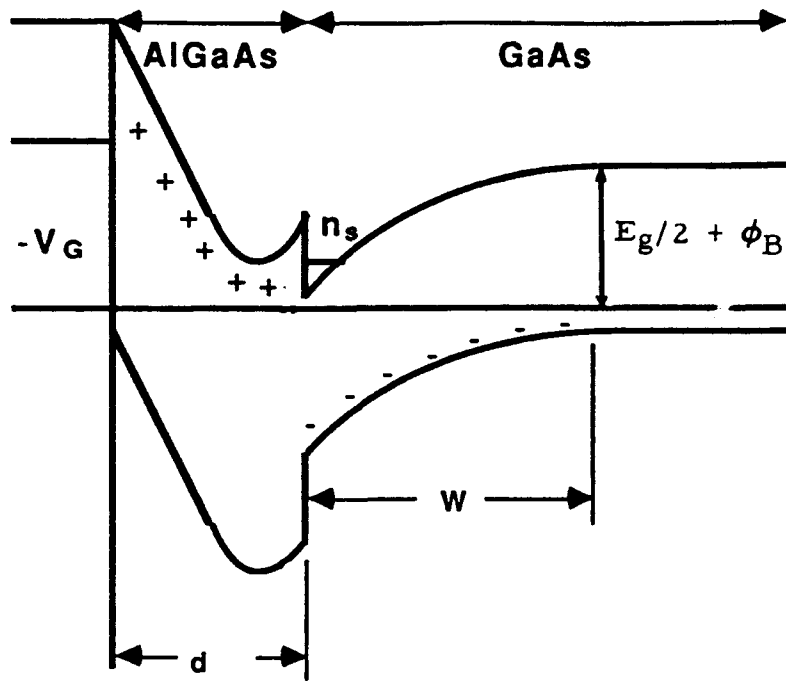


(a)

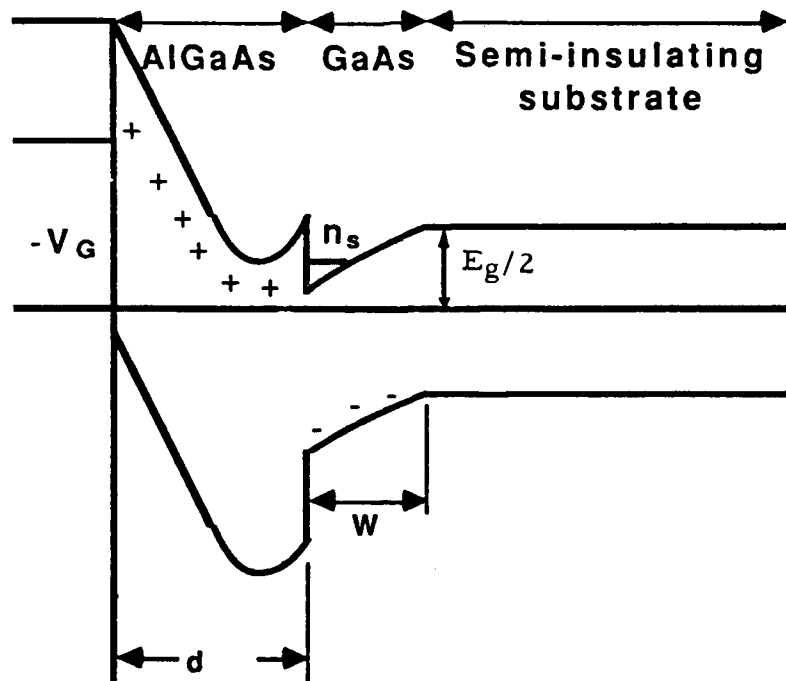


(b)

Figure 1. Schematic Cross-Section of (a) a Typical AlGaAs/GaAs HEMT and (b) a Typical SOI MOSFET



(a)



(b)

Figure 2. Band Diagram of (a) a Conventional Thick GaAs Film AlGaAs/GaAs HEMT and (b) a Thin GaAs Film AlGaAs/GaAs HEMT Terminated on a Semi-Insulating Substrate

with a Schottky barrier  $\phi_m$  at the gate and a doped AlGaAs layer of thickness  $d$ . Donor doping  $N_d$  in the AlGaAs layer and acceptor doping  $N_a$  in the active GaAs layer are assumed to be constant. In the depletion-layer approximation both donors and acceptors are assumed to be completely ionized.

The edge of the depletion region in the conventional HEMT model is defined as the point at which both the net charge and the electric field are zero. The depletion width is the distance from the AlGaAs/GaAs interface to the edge of the depletion region. It has been shown [2] that the depletion width in such a structure is

$$W = [(4\epsilon\phi_B/N_aq)]^{1/2} \quad (1)$$

where

- $\epsilon$  = the AlGaAs (GaAs) permittivity (these are assumed to be equal)
- $q$  = the elemental charge
- $\phi_B$  = the GaAs bulk potential  $[-(kT/q)\ln(N_a/n_i)]$
- $kT/q$  = the thermal voltage, and
- $n_i$  = the intrinsic carrier concentration ( $1.79 \times 10^6 \text{ cm}^{-3}$ ).

For typical values of HEMT acceptor doping, the depletion width given by Eq. (1) may exceed the GaAs film thickness. For example, an acceptor doping density of  $1 \times 10^{14} \text{ cm}^{-3}$  yields a depletion width of greater than  $3.0 \text{ }\mu\text{m}$ , which exceeds the width of the active region in thin AlGaAs/GaAs HEMTs [3]. The band diagram shown in Figure 2b is more representative of the situation in thin-layer HEMT structures. The active region, whose depth is on the order of a micron or less, is fully depleted. Therefore, the field in the active layer is finite at the semi-insulating boundary.

The electrical properties of the semi-insulating GaAs substrate are dominated by mid-level traps [22]. Therefore, in this analysis we assume

that the high density of mid-gap traps in the semi-insulating substrate is large enough to pin the Fermi level at mid-gap at the semi-insulating boundary. In the following sections we show how the finite thickness of the fully depleted GaAs active layer and the influence of Fermi level pinning at the semi-insulating interface affect the threshold characteristics of HEMTs. We then compare the threshold characteristics of the fully depleted, pinned HEMT model with the conventional HEMT (a semi-infinite active layer) and a classical MOSFET threshold analysis.

## 2. SINGLE-SUBBAND, QUANTUM-MECHANICAL HEMT MODEL

The potential across the structures shown in Figures 2a and 2b, for the conventional and finite GaAs active-layer HEMTs, respectively, may be derived from Poisson's equation to give

$$V_g = V_0 - E_f + dE_i \quad (2)$$

where

$$V_0 = \phi_m - \Delta E_c - qN_d d^2/2,$$

$$E_c = \text{the AlGaAs/GaAs conduction-band offset, and}$$

$$E_i = \text{the field at the AlGaAs/GaAs interface.}$$

Thus, for given values of the AlGaAs thickness  $d$  and donor doping  $N_d$  any difference between the gate voltages for the semi-infinite structure and the finite (pinned) structure is determined only by the differences in the Fermi levels and in the fields at the interface.

In the single-subband model [2], the Fermi level  $E_f$  is given by

$$E_f = -E_0 - (kT/q)\ln(n_s/n_c) \quad (3)$$

where

$$E_0 = \text{the first quantum level in the two-dimensional well,}$$

$$n_s = \text{the channel charge density at threshold, and}$$

$$n_c = \frac{\pi^2}{m_1} kT \text{ (where } h \text{ is Planck's constant divided by } 2\pi \text{ and } m_1 \text{ is the longitudinal effective mass of the carriers).}$$

In the triangular well approximation the first quantum level is given by:

$$E_0 = C_1[(\epsilon/q)E_i]^{2/3} \quad (4)$$

where

$$C_1 = (9\hbar^2/8m_1q)(4q^2m_1/\hbar^2\epsilon)^{2/3}.$$

Substituting Eqs. (3) and (4) into Eq. (2) yields the gate voltage in either structure in terms of the electric field evaluated at the interface and the mobile channel charge  $n_s$ .

### 3. THRESHOLD VOLTAGE

#### 3.1 CONVENTIONAL HEMT

The threshold analysis of the conventional HEMT structure has shown that for a two-dimensional, strong-inversion charge definition of threshold,  $n_s$  at threshold is (from [2])

$$n_{th} = (q/\epsilon)^{1/3} C_2 N_a / E_i^{1/3} \quad (5)$$

where

$$C_2 = (27\pi^2 \epsilon / 4 q^2 m_1)^{1/3}$$

and

$W$  = the width of the depletion layer [given by Eq. (1)].

This definition of threshold for the HEMT is equivalent to the strong-inversion definition for the MOSFET. Integrating Poisson's equation from the AlGaAs/GaAs interface to the edge of the depletion region (where the electric field is zero) and neglecting the channel charge at threshold (which is small compared to the depletion layer charge) yields

$$E_i = (q/\epsilon) N_a W_{un}. \quad (6)$$

where the subscript "un" denotes the depletion width for the conventional unpinned structure.

Combining Eqs. (1) through (6) yields the threshold voltage for the unpinned HEMT structure:

$$\begin{aligned} V_{un} = V_0 + (kT/q) \ln [C_2 (N_a^{2/3} / W_{un}^{1/3} n_c)] \\ + C_1 (N_a W_{un})^{2/3} + d(q/\epsilon) N_a W_{un} \end{aligned} \quad (7)$$

### 3.2 COMPARISON WITH THIN, FULLY DEPLETED HEMT

In the thin, fully depleted structure at threshold, the single-subband model yields the same dependence (as the conventional HEMT) on the field at the AlGaAs/GaAs interface  $E_i$  for the Fermi level  $E_f$  and for the first quantum level  $E_0$ . Therefore, any difference between the threshold voltage for the conventional structure and that of the pinned structure is due to the difference in the field at the interface. Using  $E_{un}$  and  $E_p$  to denote the fields at the interface for the unpinned structure and the pinned structure, respectively, the difference between the unpinned and pinned threshold voltage (assuming the same AlGaAs thickness and donor doping) is

$$\Delta V_{th} = (kT/3q) \ln(E_p/E_{un}) + C_1(N_a W_{un})^{2/3} [1 - (E_p/E_{un})^{2/3}] + dE_{un}(1 - E_p/E_{un}) \quad (8)$$

Integrating Poisson's equation from the AlGaAs/GaAs interface to the back surface (where the potential is pinned at  $E_g/2$ ) yields the following for the field at the AlGaAs/GaAs interface in the pinned structure:

$$E_p = (q/\epsilon) N_a W_0/2 + \phi_B/W_0 \quad (9)$$

where

$W_0$  = the length of the GaAs active region.

The solid curve in Figure 3 shows the difference in the threshold voltage between the unpinned and pinned structures versus acceptor doping as calculated by Eq. (8), assuming an AlGaAs layer thickness of 500 Å and a GaAs active-layer thickness,  $W_0$ , of 0.5 μm. As is apparent, the threshold voltage for the pinned structure can vary appreciably, by 75 mV or more, from the threshold voltage as calculated for the conventional HEMT. At very low acceptor densities ( $\sim 10^{10} \text{ cm}^{-3}$ ) the difference is only a few millivolts. However, for typical acceptor densities ( $\sim 10^{13}$  to  $10^{15} \text{ cm}^{-3}$ )

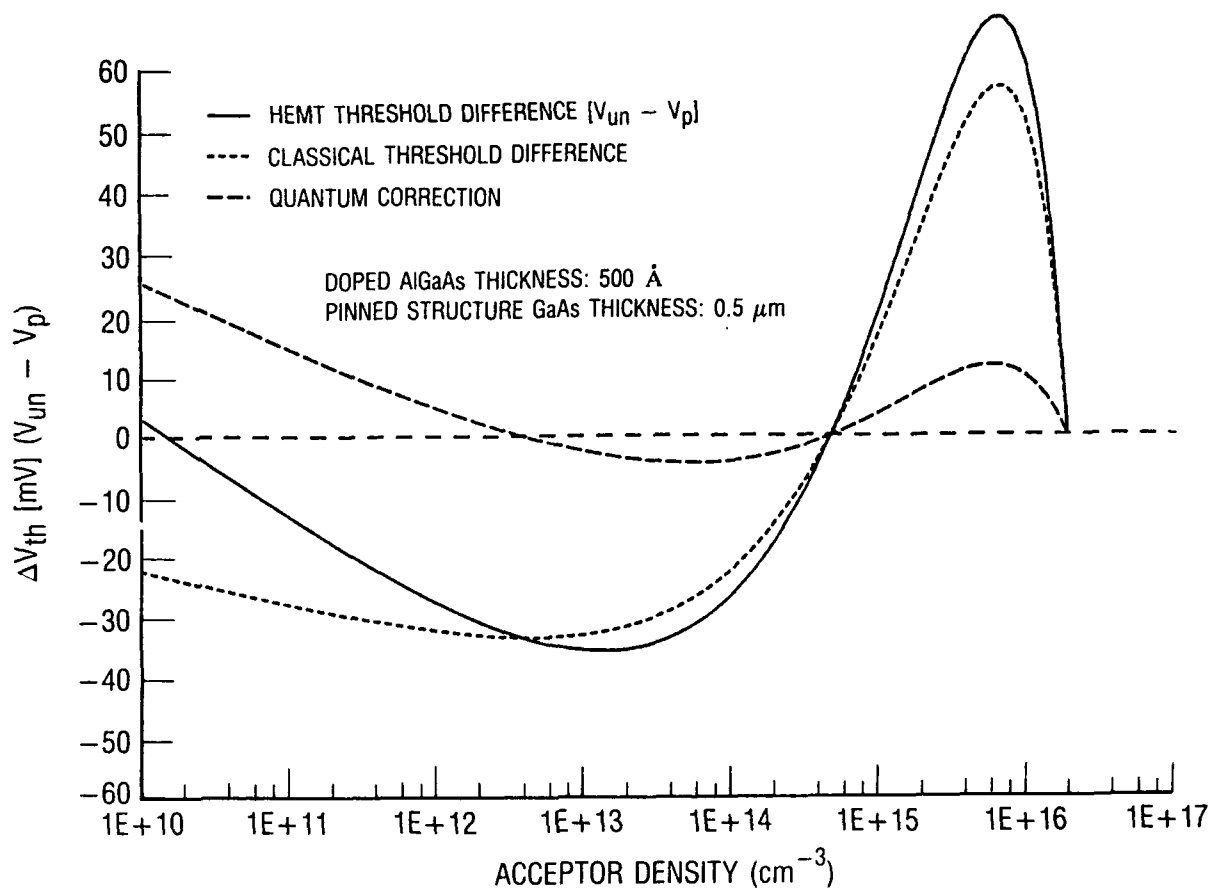


Figure 3. HEMT Threshold Voltage Difference [Unpinned Minus Pinned] vs Acceptor Density (Solid Curve). The classical contribution (as explained in the text) is shown by the small dashes. The quantum correction is shown by the long dashes.

this difference can exceed 35 mV. At relatively high acceptor densities ( $>10^{15} \text{ cm}^{-3}$ ) the threshold-voltage difference changes sign and approaches 75 mV.

For large acceptor doping densities or large GaAs active layer thicknesses, the carrier channel becomes uncoupled from the effects of the semi-insulating substrate. This occurs when the GaAs active-layer thickness exceeds the sum of the two depletion widths formed at the AlGaAs/GaAs surface and at the GaAs/semi-insulating surface, i.e., when

$$W_{\text{max}} = W_{\text{un}} + W_1 \quad (10)$$

where,  $W_{\max}$  is the maximum GaAs active-layer thickness,  $W_{\text{un}}$  is calculated as before, and  $W_1$  is calculated in the depletion layer approximation for band bending of  $\phi_B$ . The result can be conveniently written in terms of  $W_{\text{un}}$ :

$$W_{\max} = (1 + 1/\sqrt{2}) W_{\text{un}} \quad (11)$$

Figure 4 shows  $W_{\max}$  versus acceptor density. For large active layers or large acceptor densities, the conventional, semi-infinite analysis of HEMT threshold characteristics is valid. However, for the smaller active layers and acceptor densities found in thin GaAs microcircuits, the effects of pinning on device characteristics must be taken into account.

The difference in the threshold voltage versus acceptor density for various GaAs active layer widths is shown in Figure 5. For a width of 0.8  $\mu\text{m}$ , the threshold voltage shows a discrepancy of a few tens of millivolts over the whole range of acceptor densities. The greatest discrepancy for the 0.8  $\mu\text{m}$  structure occurs just before the difference in the threshold voltage falls to zero (at  $\sim 1 \times 10^{16} \text{ cm}^{-3}$ ) as the front and back interfaces become uncoupled. As the GaAs layer shrinks, the discrepancy increases between the threshold voltage analyses of the conventional and the pinned structures, and the range over acceptor densities for which the pinned analysis is applicable also increases. When the active-layer dimensions reach 0.2  $\mu\text{m}$ , the discrepancy between the pinned and unpinned analyses is near -125 mV at typical acceptor densities ( $\sim 10^{14} \text{ cm}^{-3}$ ) and exceeds 175 mV for acceptor densities near  $1 \times 10^{17} \text{ cm}^{-3}$ .

The effect of shrinking device dimensions is clearly seen in Figure 6, in which the threshold-voltage discrepancy versus the GaAs active-layer width is plotted for various acceptor densities. For small active-layer widths (0.1 to 1.0  $\mu\text{m}$ ) the threshold-voltage discrepancy can be as great as -250 mV at typical acceptor densities ( $1 \times 10^{14} \text{ cm}^{-3}$ ), or it can be of opposite sign and as great as 100 mV at large acceptor densities ( $1 \times 10^{16} \text{ cm}^{-3}$ ).

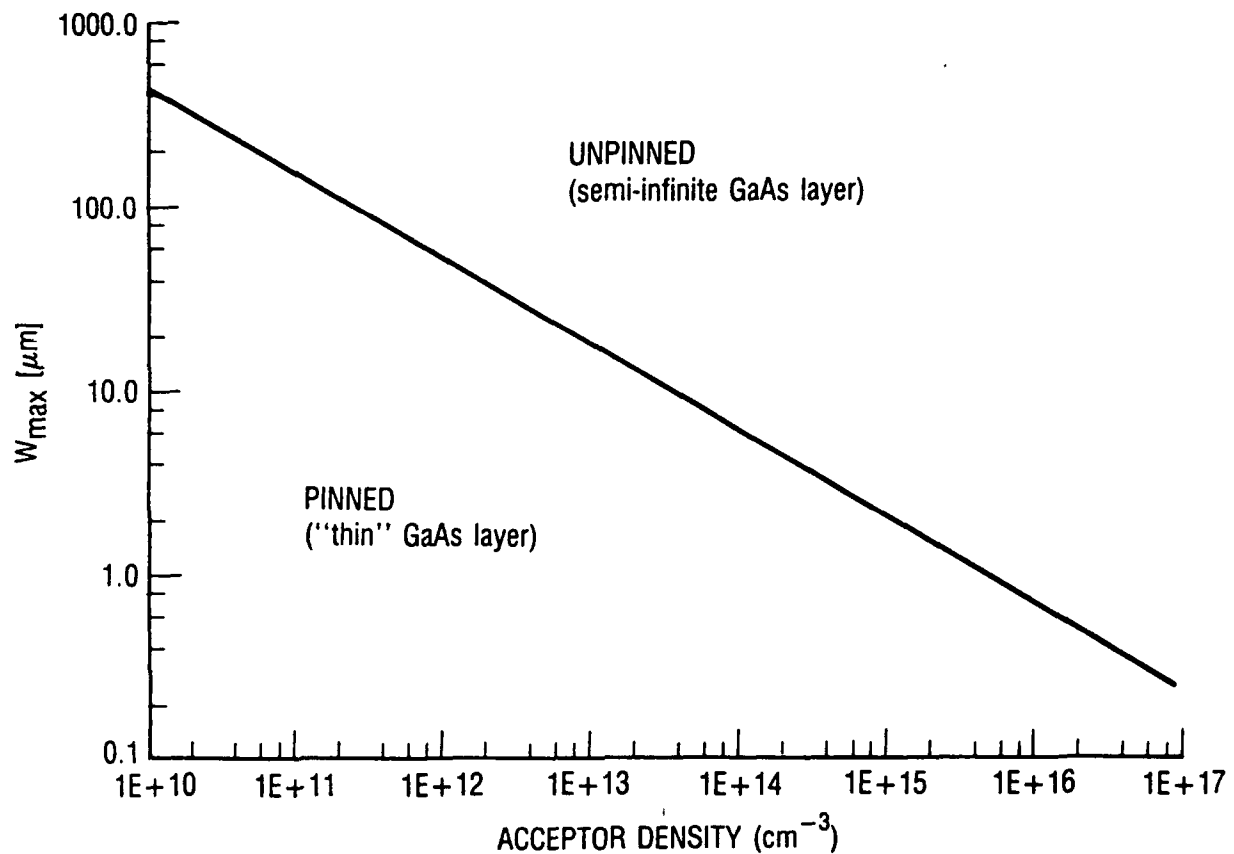


Figure 4. The Maximum GaAs Active-Layer Width  $W_{\max}$  (for Which the Carrier Channel is Coupled to the Back, Semi-Insulating Surface) vs Acceptor Density. Structures with large GaAs layers and large acceptor densities are uncoupled and the conventional, semi-infinite analysis is valid. For thin GaAs microcircuits the analysis that includes communication between the interfaces must be applied.

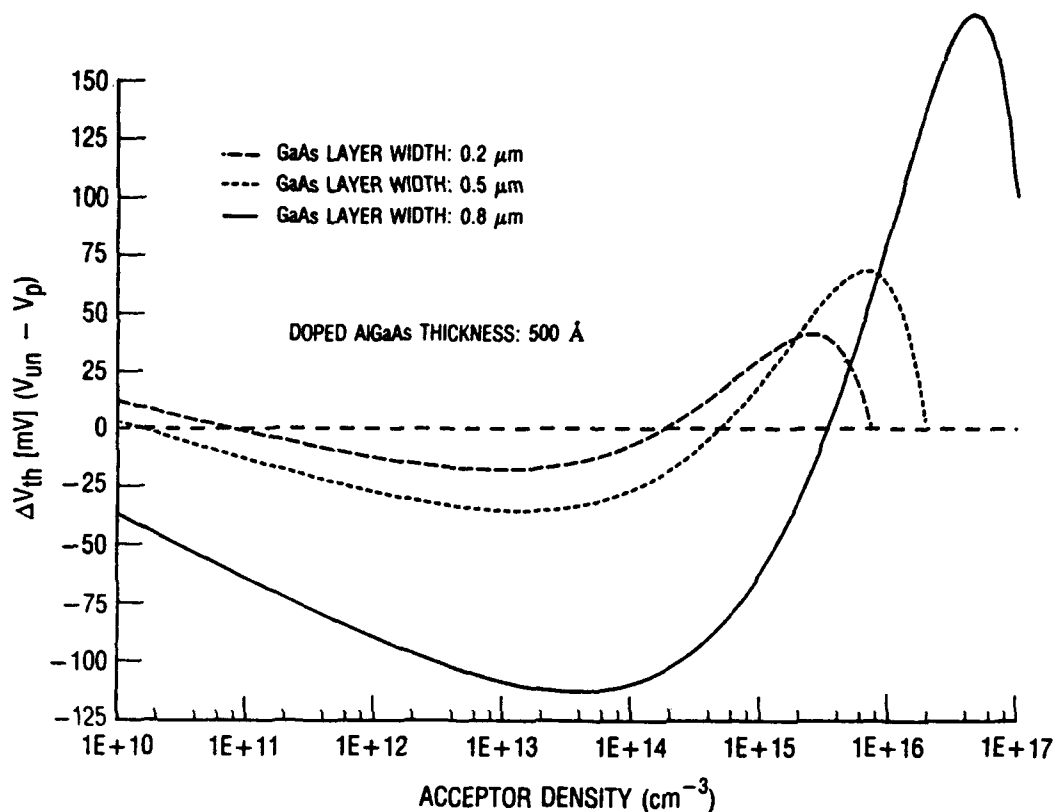


Figure 5. Difference in HEMT Threshold Voltage [Unpinned Minus Pinned] vs Acceptor Density for Various GaAs Active-Layer Thicknesses

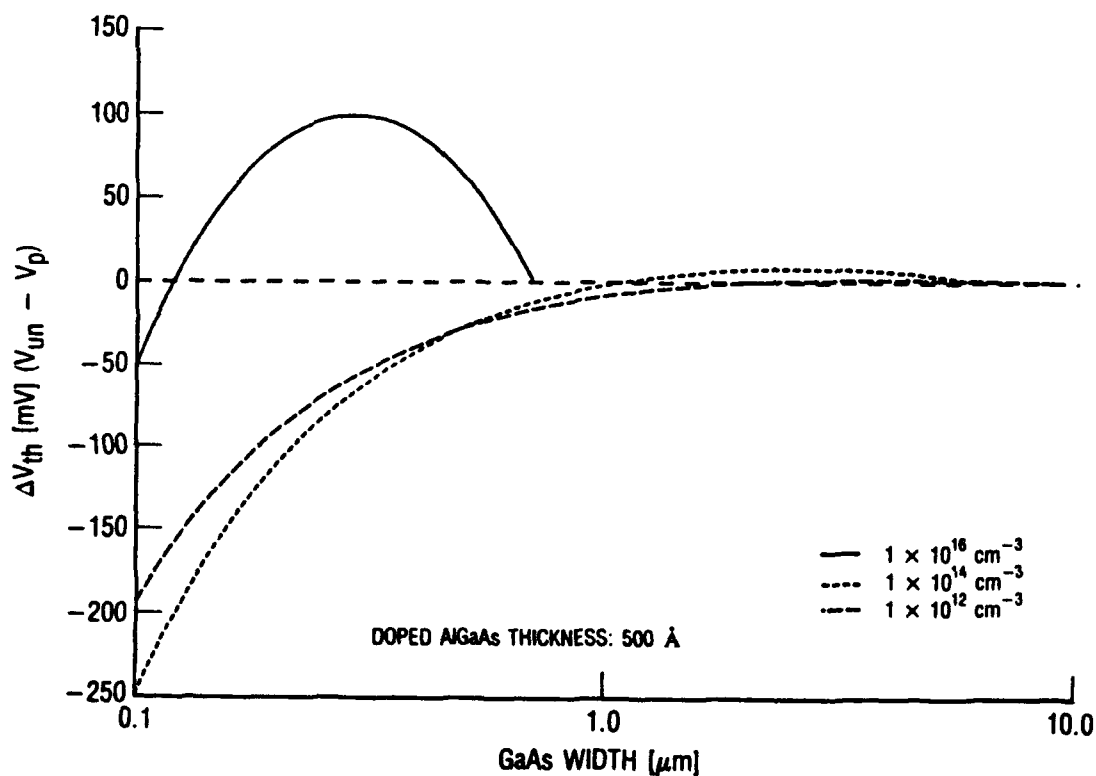


Figure 6. Difference in HEMT Threshold Voltage [Unpinned Minus Pinned] vs GaAs Active-Layer Width for Various Acceptor Densities

#### 4. COMPARISON WITH A CLASSICAL ANALYSIS OF MOSFET THRESHOLD

Recently [23], a classical analysis of the channel electron concentration was compared to various two- and three-dimensional quantum mechanical approximations of this concentration. Therefore, we have studied the discrepancy between our two-dimensional, strong-inversion threshold model and the classical analysis of the pinned and unpinned structures.

In the classical MOSFET analysis the threshold voltage is defined as the gate voltage at which the surface band bending is at some predetermined value, such as twice the bulk potential. This definition equates the surface-carrier concentration to the majority-carrier concentration in the bulk. A similar classical definition may be invoked for the HEMT.

Since by this definition the Fermi level  $E_f$  at threshold is the same for both the pinned and unpinned structures, the difference between the classical threshold voltages for the two structures is found from Eq. (7) to be

$$\Delta V_{cl} = dE_{un} (1 - E_p/E_{un}) \quad (12)$$

where  $E_p$  and  $E_{un}$  are defined as before. Therefore, the difference between the quantum and classical threshold-voltage descriptions is due only to the difference in the Fermi levels (surface potentials) at threshold. Therefore, the threshold-voltage difference in Eq. (8) may be written in the following form:

$$\Delta V_{th} = \Delta V_{cl} + \Delta V_{qm} \quad (13)$$

where the quantum correction,  $\Delta V_{qm}$ , is given by

$$\Delta V_{qm} = (kT/3q) \ln(E_p/E_{un}) + C_1(N_a W_{un})^{2/3} [1 - (E_p/E_{un})^{2/3}] \quad (14)$$

Figure 3 illustrates the classical and quantum components of the difference in the threshold voltages for the unpinned and pinned HEMT structures versus acceptor doping. For low acceptor densities the classical results differ significantly from the quantum results and have different signs. As the acceptor density increases above about  $10^{12} \text{ cm}^{-3}$ , the quantum correction falls below 10 mV.

In Figure 7 the threshold-voltage difference is plotted versus the GaAs active-layer width for an acceptor density of  $1 \times 10^{14} \text{ cm}^{-3}$  and an AlGaAs thickness of 500 Å. A large difference in the threshold voltage appears as the GaAs active-layer thickness decreases. Even at 0.3 μm, which is well within the capability of present technology [3], the threshold-voltage difference is almost 100 mV. At an acceptor doping density of  $1 \times 10^{14} \text{ cm}^{-3}$ , the quantum correction is relatively small compared to the classical results over the whole range of GaAs widths shown. As the acceptor density decreases from this value and GaAs widths decrease, this difference can increase as shown in Figure 3.

Note the several parameter values in Figures 3 and 7 that yield the same threshold-voltage values for the pinned and unpinned structures, i.e., where  $V_{th} = 0$ . For low values of the acceptor density, the quantum-mechanical correction can become large and of opposite sign from the classical component. At  $N_a = 2 \times 10^{10} \text{ cm}^{-3}$  in Figure 3, the effective cancellation of these terms yields one zero. As the acceptor concentration increases, a second zero occurs at  $N_a = 5 \times 10^{14} \text{ cm}^{-3}$  in Figure 3. At this point the fields at the AlGaAs/GaAs interface are identical in the pinned and unpinned structures. Hence, both the classical and the quantum-mechanical components of the threshold-voltage difference fall to zero.

The zero at the largest acceptor density occurs when the two-dimensional channel at the AlGaAs/GaAs interface becomes uncoupled from the back semi-insulating GaAs interface. For acceptor densities greater than this the device may be analyzed as if it were a conventional, semi-infinite structure. The ramifications of this result are discussed Section 5.

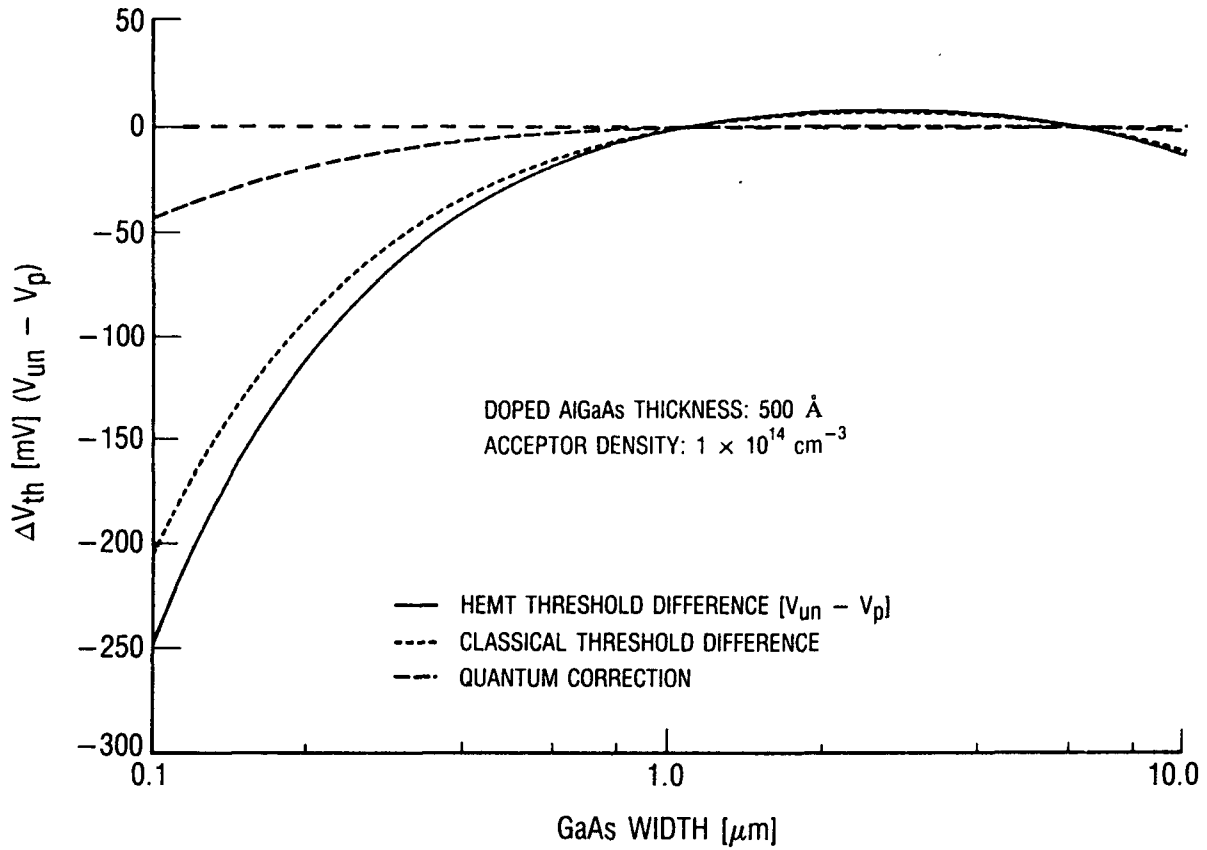


Figure 7. Difference in HEMT Threshold Voltage [Unpinned Minus Pinned] vs GaAs Active-Layer Thickness in the Pinned Structure. The classical contribution is shown by the small dashes. The quantum-mechanical correction is shown by the long dashes.

## 5. SHAPE OF THE CONDUCTION BAND

The pinning of the Fermi level at the semi-insulating substrate affects the overall shape of the conduction-band edge as well as the threshold voltage. The integration of Poisson's equation from the AlGaAs/GaAs interface into the active layer yields the potential of the conduction-band edge, relative to the Fermi level, as a function of its position across the structure. The results of this calculation for the conventional, unpinned structure and the pinned structure are given by

$$-V_{un}(x) = E_F + 4 \phi_B(x/W_{un}) (1 - x/2W_{un}) \quad (15)$$

and by

$$-V_p(x) = E_g/2 + \phi_B(x/W_0 - 1) + (q/\epsilon)(N_a W_0^2/2)(x/W_0)(1 - x/W_0) \quad (16)$$

where  $x$  is the position in the active layer relative to the AlGaAs/GaAs interface and, for convenience, the negative value of the conduction band potential (i.e. the conduction band energy) has been given.

In Figures 8 and 9 the conduction-band edge in the pinned HEMT structure is plotted versus the relative position in the active layer for three active layer thicknesses at two different acceptor densities, respectively. For each doping density the position of the conduction-band edge for the semi-infinite structure has also been included. For the pinned devices the position is normalized to the GaAs active-layer thickness  $W_0$ , while for the unpinned structure the position is normalized to the depletion width  $W_{un}$  (which may be very much larger than the active-layer thickness of the pinned devices). Although it appears that the conduction-band edges are coincident at the AlGaAs/GaAs interface in Figure 8, there is a slight difference in the value of the potential at this interface. This small difference results because in the two-dimensional quantum-well model of threshold the position of the Fermi level must change to maintain a constant value of the strong-inversion charge in each case.

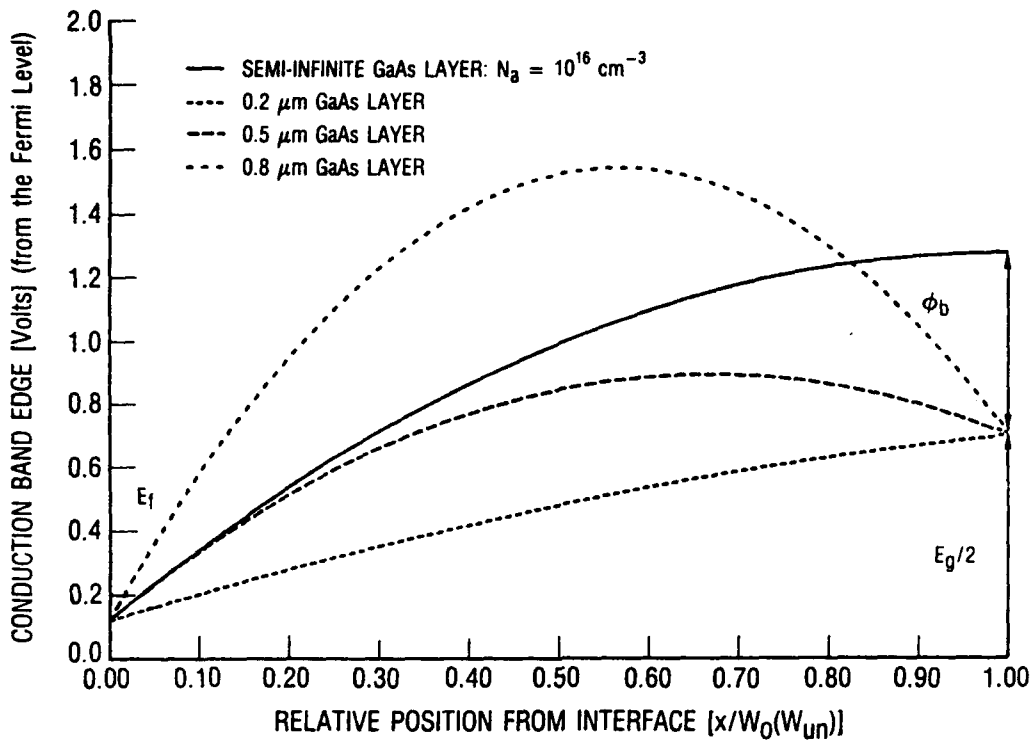


Figure 8. The Conduction-Band Edge Relative to the Fermi Level vs Relative Position in the Active Layer for Various Active-Layer Widths and Acceptor Densities of  $1 \times 10^{16} \text{ cm}^{-3}$

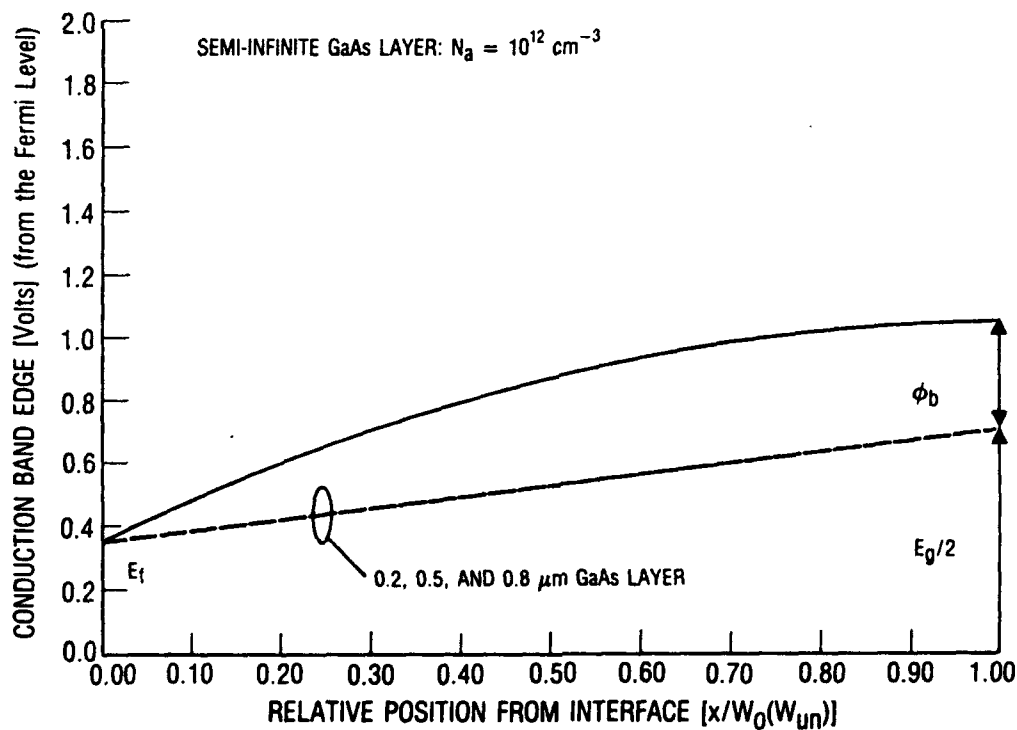


Figure 9. The Conduction-Band Edge Relative to the Fermi Level vs Relative Position in the Active Layer for Various Active-Layer Widths and Acceptor Densities of  $1 \times 10^{12} \text{ cm}^{-3}$

At the semi-insulating boundary, the conduction bands of the pinned structures all meet at the same potential,  $E_g/2$ , which is  $\phi_B$  below the value for the conduction band in the unpinned structures at the depletion edge. The pinning of the Fermi level at mid-gap at the semi-insulating boundary gives rise to the communication between the carrier channel and the semi-insulating boundary. For a relatively large acceptor density ( $1 \times 10^{16} \text{ cm}^{-3}$  in Figure 8) the shape of the conduction band shows a nearly constant field for the  $0.8 \text{ }\mu\text{m}$  GaAs active-layer structures. The shorter ( $0.2 \text{ }\mu\text{m}$ ) structure shows a relatively large positive field at the AlGaAs/GaAs interface; this field decreases to zero in the active layer and is large and negative at the semi-insulating interface. The results for the  $0.5 \text{ }\mu\text{m}$  structure, also plotted in Figure 8, show that the curvature of the conduction-band edge changes smoothly with GaAs active-layer thickness.

For comparison, in Figure 9 the conduction-band edge versus relative position in the active layer is plotted for a relatively small acceptor density ( $1 \times 10^{12} \text{ cm}^{-3}$ ). At this low value of acceptor density, the field across the pinned structure is virtually constant for all the GaAs active-layer widths plotted.

The conduction-band edge versus relative active-layer position is plotted in Figure 10 for an active-layer thickness of  $0.8 \text{ }\mu\text{m}$  for the acceptor densities shown. At the AlGaAs/GaAs interface, the conduction-band edge moves closer to the Fermi level with increasing acceptor density, in keeping with the two-dimensional, strong-inversion definition of threshold as discussed above. All three curves terminate at  $E_g/2$  at the semi-insulating boundary. For the lowest acceptor density ( $1 \times 10^{12} \text{ cm}^{-3}$ ), the field across the structure (represented by the slope of the conduction-band edge) is virtually constant. As the acceptor doping increases (to  $1 \times 10^{14} \text{ cm}^{-3}$ ) the field remains relatively constant, but increases somewhat at the AlGaAs/GaAs interface and decreases slightly at the semi-insulating boundary. For the largest doping density ( $1 \times 10^{16} \text{ cm}^{-3}$ ), the field at the AlGaAs/GaAs interface becomes very large and the field at the semi-insulating boundary changes sign and also becomes large. Similar behavior in the conduction band is seen for thinner structures.

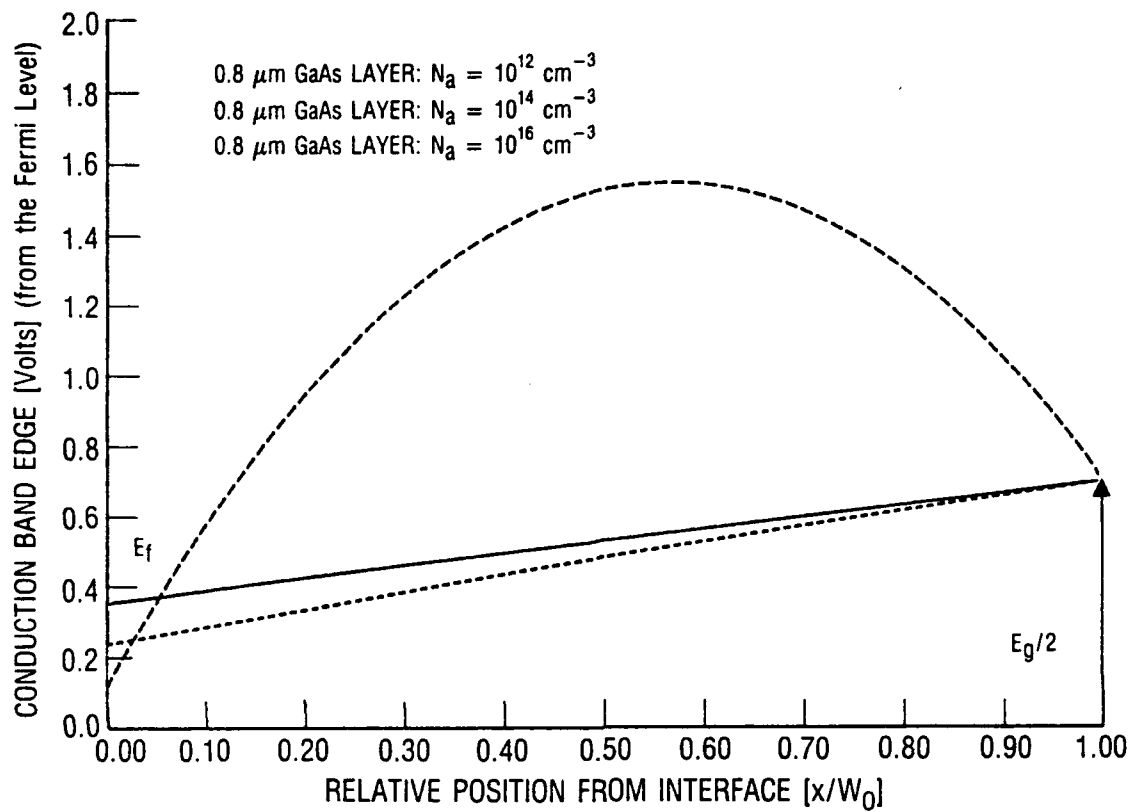


Figure 10. The Conduction-Band Edge Relative to the Fermi Level vs Relative Position in the Active Layer for the 0.8 μm Structure and Various Acceptor Dopings

## 6. SUMMARY

The effects of the pinning of the Fermi level at the back interface of AlGaAs/GaAs high-electron-mobility transistors have been investigated; this pinning is due to large mid-gap trap densities in the semi-insulating GaAs substrate. We have shown that the back semi-insulating boundary can have a significant effect on the free-carrier density at the AlGaAs/GaAs interface, and that the effect of the semi-insulating interface on the threshold voltage becomes more pronounced as the GaAs active layer decreases. Such effects cannot be ignored for the lightly doped active-layer structures being used in thin GaAs microcircuits.

A triangular-well, single-subband, quantum-mechanical analysis of the threshold voltage of these fully depleted, pinned structures has been developed and compared to the results for the unpinned, semi-infinite structures. These quantum-well results have also been compared to the results obtained by a classical analysis of threshold voltage. It has been shown that quantum effects for the pinned structures are more important as device dimensions shrink, and these effects are particularly important as doping densities decrease. In fact, for the triangular-well model at low acceptor densities, the quantum component of the difference in the threshold voltage between unpinned and pinned structures is large and of the opposite sign compared to the results of the classical analysis.

The effects of Fermi-level pinning on the shape of the conduction band in the active GaAs layer have also been described. We have shown that for thin structures (with an active layer thickness of  $0.2\text{ }\mu\text{m}$ ), the field in the active layer is roughly constant for all doping densities in the microcircuits of interest. For larger structures (with active-layer thicknesses of up to  $0.8\text{ }\mu\text{m}$ ) substantial band bending occurs. For large acceptor densities (approaching  $1 \times 10^{16}\text{ cm}^{-3}$ ) the field in the active layer can be large and positive at the AlGaAs/GaAs interface, decrease to zero in the interior of the active layer, and become large and negative at the semi-insulating boundary.

## REFERENCES

1. R. J. Krantz and W. L. Bloss, "Subthreshold I-V Characteristics of AlGaAs/GaAs MODFETs: The Role of Unintentional Acceptors," accepted for publication, IEEE Trans. El. Dev. (Nov. 1989).
2. R. J. Krantz and W. L. Bloss, "The Role of Unintentional Acceptor Concentration on the Threshold Voltage of Modulation-Doped Field-Effect Transistors," IEEE Trans. El. Dev. vol. ED-36, pp. 451-453 (Feb. 1989).
3. B. K. Janousek, R. J. Krantz, W. L. Bloss, W. E. Yamada, S. Brown, R. Remke, and S. Witmer, "Characteristics of GaAs Heterojunction FETs (HFETs) and Source Follower FET Logic (SFFL) Inverters Exposed to High Energy Neutrons," accepted for publication, IEEE Trans. Nuc. Sci. (Dec. 1989).
4. D. Delagebeaudeuf and N. T. Linh, "Metal-(n) AlGaAs-GaAs Two-Dimensional Electron Gas FET," IEEE Trans. El. Dev. vol. ED-29, pp. 955-960 (June 1982).
5. J. Baek, M. S. Shur, R. R. Daniels, D. K. Arch, J. K. Abrokwhah, and O. N. Tufte, "Current-Voltage and Capacitance-Voltage Characteristics of Heterojunction Insulated-Gate Field-Effect Transistors," IEEE Trans. El. Dev. vol. ED-34, pp. 1650-1657 (August 1987).
6. W. A. Hughes and C. M. Snowden, "Nonlinear Charge Control in AlGaAs/GaAs Modulation-Doped FETs," IEEE Trans. El. Dev. vol. ED-34, pp. 1617-1625 (August 1987).
7. C. Chang and H. R. Fetterman, "An Analytic Model for HEMTs Using New Velocity-Field Dependence," IEEE Trans. El. Dev. vol. ED-34, pp. 1456-1462 (July 1987).
8. D. H. Lee and S. S. Li, "Effects of DX Center and Spatial Distribution of Electrons on the Density of Two-Dimensional Electron Gas in Modulation-Doped AlGaAs/GaAs Heterojunction Structure," J. App. Phys. vol. 60, pp. 3789-3791 (15 Nov. 1986).
9. Y. M. Kim and P. Roblin, "Two-Dimensional Charge-Control Model for MODFETs," IEEE Trans. El. Dev. vol. ED-33, pp. 1644-1651 (Nov. 1986).
10. A. A. Grinberg, "The Effect of the Two-Dimensional Gas Degeneracy of the I-V Characteristics of the Modulation-Doped Field-Effect Transistor," J. Appl. Phys. vol. 60, pp. 1097-1103 (1 August 1986).
11. L. P. Sadwick and K. L. Wang, "A Treatise on the Capacitance-Voltage Relation of High Electron Mobility Transistors," IEEE Trans. El. Dev. vol. ED-33, pp. 651-656 (May 1986).

12. B. Vinter, "Subbands and Charge Control in a Two-Dimensional Electron Gas Field-Effect Transistor," Appl. Phys Lett. vol. 44, pp. 307-309 (1 Feb. 1984).
13. K. Lee and M. Shur, "Electron Density of the Two-Dimensional Electron Gas in Modulation Doped Layers," J. Appl. Phys. vol. 54, pp. 2093-2096, Apr. 1983.
14. T. J. Drummond, H. Morkoc, K. Lee, and M. S. Shur, "Model for Modulation Doped Field-Effect-Transistors," IEEE El. Dev. Lett. vol. EDL-3, pp. 338-341 (Nov. 1982).
15. Y. Omura, S. Nakashima, and K. Izumi, "Theoretical Analysis on Threshold Characteristics of Surface-Channel MOSFETs Fabricated on a Buried Oxide," IEEE Trans. El. Dev. vol. ED-30, pp. 1656-1662 (Dec. 1983).
16. H. -K. Lim and J. G. Fossum, "Threshold Voltage of Thin-Film Silicon-on-Insulator (SOI) MOSFETs," IEEE Trans. El. Dev. vol. ED-30, pp. 1244-1251 (Oct. 1983).
17. E. R. Worley, "Theory of the Fully Depleted SOS/MOS Transistor," Solid State El. vol. 23, pp. 1107-1111 (1980).
18. D. Kranzer, K. Schluter, and D. Takacs, "Threshold Voltage Model of ESFI-SOS-MOS Transistors," IEEE Trans. El. Dev. vol. ED-25, pp. 890-894 (August 1978).
19. J. Tihanyi and H. Schlotterer, "Properties of ESFI MOS Transistors Due to the Floating Substrate and the Finite Volume," IEEE Trans. El. Dev. vol ED-22. pp. 1017-1023 (Nov. 1975).
20. K. K. Young, "Analysis of Conduction in Fully Deleted SOI MOSFETs," IEEE Trans. El. Dev. vol. 36, pp. 504-506 (March 1989).
21. M. Yoshimi, H. Hazama, M. Takahashi, S. Kambayashi, T. Wada, K. Kato, and H. Tango, "Two-Dimensional Simulation and Measurement of High-Performance MOSFETs Made on a Very Thin SOI Film," IEEE El. Dev. vol. 36, pp. 493-503 (March 1989).
22. P. F. Lindquist and W. M. Ford, "Semi-insulating GaAs Substrates," in GaAs FET Principles and Technology, Ch. 1, eds. J.V. DiLorenzo and D. D. Khandelwal, Artech House, Mass. (1982).
23. J. Yoshida, "Classical Versus Quantum Mechanical Calculation of the Electron Distribution at the n-AlGaAs/GaAs Heterointerface," IEEE Trans. El. Dev. vol. ED-33, pp. 154-156 (Jan. 1986).